hamedov.[34] Boiteux and Hess considered the glycolysis reaction while Holmuhamedov studied a mitochondrial suspension. Both systems were excitable. Under certain conditions in a thin layer, standing mosaic patterns were observed and the contrast of the structures periodically changed.

The onset of a chaos in chemical systems has been extensively investigated for the last decade (Swinney and Roux,[35] Maselko and Swinney,[36] and references therein), and both experimental and theoretical techniques for such studies were significantly advanced there. However, all these papers considered purely temporal (well-stirred) systems and even if spatial effects were taken into account, they were considered from the point of view of a possible source of noise or artifacts. Diffusion-induced chaos was considered theoretically by Kuramoto and Yamada[37,38] and Rössler[39] with rather abstract models of locally oscillating system. Apparently, the present work is the first prediction of diffusion-induced chaos in a real chemical system. It also demonstrates that transition to chaos can occur immediately from a stationary state and that chaos and a stationary state may even coexist. So, a series of bifurcations from a steady state to chaos is not always a prerequisite of chaotic phenomena.

Although the calculations were performed with a very coarse discretization, there is no reason to doubt the results. The discretization of a PDE system simplifies the problem in a sense, and one may believe that a further increase of the density of the mesh points will not only retain the complex attractive set but also make it more easily detectable.

The principal question is how these results concern experiments. Although there is a hint that this kind of behavior was observed in the Belousov-Zhabotinsky medium,[32] there is no clear evidence that it has been observed in this or any other system. The model predicts that the onset of an irregular spatio-temporal regime in the Belousov-Zhaboinsky medium should strongly depend on the diffusibilities of the species involved. It is a difficult task to control diffusion in this system and it is much more complicated if there is a need to vary the diffusion coefficients of different species selectively. Therefore, one could hardly expect that these structures would be found easily. However, further theoretical examination of the probem can, probably, suggest more convenient routes for an experimental approach.

The fact that phenomena like these are described by a rather simple realistic model of a well-known chemical reaction at reasonable values of the essential parameters should stimulate the studies of the spatio-temporal periodic patterns in chemical systems and should facilitate a deeper insight into its nature and role in self-organization processes.

*Acknowledgment.* The author is grateful to Prof. A. M. Zhabotinsky and Drs. Yu. A. Kuznetzov and A. N. Zaikin for useful discussions.

**Registry No.** $BrO_3$, 15541-45-4; $Fe(phen)_3^{2+}$, 14708-99-7; $CHBr(COOH)_2$, 600-31-7.

(33) Boiteux, A.; Hess, B. B. *Ber. Bunsen-Ges. Phys. Chem.* **1980**, *84*, 392-398.
(34) Holmuhamedov, E. L. *Eur. J. Biochem.* **1986**, *158*, 543-546.
(35) Swinney, H. L.; Roux, J. C. In *Non-Equilibrium Dynamics in Chemical Systems*; Vidal, C., Pacault, A., Eds.; Springer Series in Synergetics; Springer-Verlag: New York, 1984.
(36) Maselko, J.; Swinney, H. L. *Phys. Scr.* **1985**, *T9*, 35-39.
(37) Kuramoto, Y.; Yamada, T. *Prog. Theor. Phys.* **1976**, *56*, 679-681.
(38) Kuramoto, Y. *Suppl. Prog. Theor. Phys.* **1978**, *64*, 346-367.
(39) Rössler, O. E. *Z. Naturforsch.* **1976**, *31A*, 1168.

# Temperature Dependence of the O + $HO_2$ Rate Coefficient

**J. M. Nicovich and P. H. Wine***

*Molecular Sciences Branch, Georgia Tech Research Institute, Georgia Institute of Technology, Atlanta, Georgia 30332* *(Received: February 2, 1987; In Final Form: May 19, 1987)*

A pulsed laser photolysis technique has been employed to investigate the kinetics of the radical-radical reaction $O(^3P) + HO_2 \xrightarrow{k_1} OH + O_2$ over the temperature range 266-391 K in 80 Torr of $N_2$ diluent gas. $O(^3P)$ was produced by 248.5-nm KrF laser photolysis of $O_3$ followed by rapid quenching of $O(^1D)$ to $O(^3P)$, while $HO_2$ was produced by simultaneous photolysis of $H_2O_2$ to create OH radicals which, in turn, reacted with $H_2O_2$ to yield $HO_2$. The $O(^3P)$ temporal profile was monitored by using time-resolved resonance fluorescence spectroscopy. The $HO_2$ concentration was calculated based on experimentally measured parameters. The following Arrhenius expression describes our experimental results: $k_1(T) = (2.91 \pm 0.70) \times 10^{-11} \exp[(228 \pm 75)/T]$ where the errors are $2\sigma$ and represent precision only. The absolute uncertainty in $k_1$ at any temperature within the range 266-391 K is estimated to be ±22%. Our results are in excellent agreement with a discharge flow study of the temperature dependence of $k_1$ in 1 Torr of He diluent reported by Keyser, and significantly reduce the uncertainty in the rate of this important stratospheric reaction at subambient temperatures.

## Introduction

The reaction of ground-state oxygen atoms with hydroperoxyl radicals

$$O(^3P) + HO_2 \rightarrow OH + O_2 \quad (1)$$

is a major odd oxygen destruction pathway in the upper stratosphere and mesosphere. Along with the reactions

$$O(^3P) + OH \rightarrow H + O_2 \quad (2)$$

$$H + O_2 + M \rightarrow HO_2 + M \quad (3)$$

$$H + O_3 \rightarrow OH + O_2 \quad (4)$$

reaction 1 plays a major role in controlling the partitioning among H, OH, and $HO_2$ radicals in the upper atmosphere. Hence, accurate kinetic data for reaction 1 are needed in order to model upper atmospheric chemistry.

Several kinetics studies of reaction 1 are reported in the literature.[1-7] Four recent direct measurements of $k_1$ at 298 K are

* Author to whom correspondence should be addressed.

(1) Burrows, J. P.; Cliff, D. I.; Harris, G. N.; Thrush, B. A.; Wilkinson, J. P. T. *Proc. R. Soc. London, A* **1979**, *368*, 463.
(2) Hack, W.; Preuss, A. W.; Temps, F.; Wagner, H. Gg. *Ber. Bunsenges. Phys. Chem.* **1979**, *83*, 1275.
(3) Lii, R. R.; Sauer, M. C., Jr.; Gordon, S. *J. Phys. Chem.* **1980**, *84*, 817.
(4) Sridharan, U. C.; Qiu, L. X.; Kaufman, F. *J. Phys. Chem.* **1982**, *86*, 4469.

0022-3654/87/2091-5118$01.50/0 

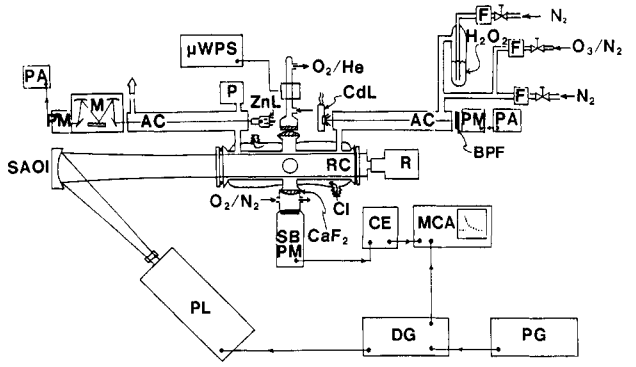


**Figure 1.** Schematic of the apparatus: AC, absorption cell; BPF, band-pass filter; CdL, cadmium lamp; CE, counting electronics; CI, coolant inlet; DG, delay generator; F, flow meter; M, monochromator; MCA, multichannel analyzer; μWPS, microwave power supply; PG, pulse generator; PA, picoammeter; P, pressure gauge; PL, photolysis laser; PM, photomultiplier; R, radiometer; RC, reaction cell; SAOI, segmented aperture optical integrator; SBPM, solar blind photomultiplier; ZnL, zinc lamp. For the sake of clarity, the solar blind photomultiplier and resonance lamp are shown at 180°. In reality, the SBPM, resonance lamp, and laser beam were at right angles to each other.

in excellent agreement,[4-7] with reported rate coefficients all within the range (5.2–6.2) × $10^{-11}$ $cm^3$ $molecule^{-1}$ $s^{-1}$. However, there has been only one investigation of the temperature dependence of $k_1$. Keyser[5] studied reaction 1 over the temperature range 229–372 K in a discharge flow system at 1-Torr total pressure and observed that $k_1(T)$ increased with decreasing temperature; his reported "negative activation energy" was ~0.4 kcal $mol^{-1}$. Although Keyser's study of reaction 1 was a high-quality experiment which appears to be free of significant systematic errors, the uncertainty in his reported activation energy will remain undesirably high[8] until independent confirmation is reported.

Several years ago, we developed a pulsed laser photolysis technique for studying the kinetics of radical–radical reactions at pressures up to 1 atm. We first applied this technique to investigate reaction 1 at 298 K over the pressure range 10–500 Torr.[6] In this paper, we report the results of a pulsed laser photolysis–resonance fluorescence study of the temperature dependence of $k_1$. Our results, obtained by using a much different experimental approach than that employed by Keyser,[5] confirm his reported temperature dependence and also demonstrate that $k_1$ is independent of pressure at subambient temperatures.

## Experimental Section

With a few modifications, the experiments were carried out in the same manner as our previous room-temperature study.[6] A review of the experimental approach, along with details pertinent to this investigation, is given below. A schematic of the apparatus is shown in Figure 1.

All experiments were carried out under slow-flow conditions using a jacketed Pyrex reactor with an internal volume of 320 $cm^3$. The cell was maintained at a constant temperature by circulating ethylene glycol from a thermostated bath through the outer jacket. A copper–constantan thermocouple with a stainless steel jacket was inserted into the reaction zone through a vacuum seal, thus allowing measurement of the gas temperature under the precise pressure and flow conditions of the experiment.

Reactants were produced with $HO_2$ in excess by 248.5-nm pulsed laser photolysis of $H_2O_2/O_3/N_2$ mixtures:

$$H_2O_2 + h\nu\ (248.5\ nm) \rightarrow 2OH \quad (5)$$

$$O_3 + h\nu\ (248.5\ nm) \rightarrow O(^1D) + O_2(a^1\Delta_g) \quad (6a)$$

$$O_3 + h\nu\ (248.5\ nm) \rightarrow O(^3P) + O_2(X^3\Sigma_g^-) \quad (6b)$$

$$OH + H_2O_2 \rightarrow HO_2 + H_2O \quad (7)$$

$$O(^1D) + N_2 \rightarrow O(^3P) + N_2 \quad (8)$$

A Lambda Physik Model 200E KrF excimer laser was used as the photolysis light source. Kinetic data were obtained by time-resolved resonance fluorescence detection of $O(^3P)$. The laser pulse width was 20 ns while, under our experimental conditions, reactions 7 and 8 proceeded at rates of (3–10) × $10^3$ and 7 × $10^7$ $s^{-1}$, respectively. $O(^3P)$ decay rates were typically in the range 30–500 $s^{-1}$.

As in our previous study, the concentration of the excess reactant, $HO_2$, was not directly measured but was calculated based on experimentally measured and other known parameters. To obtain $[HO_2]$, one must determine $[OH]_0$, the initial concentration of photolytically produced OH, and the yield of $HO_2$ from reaction 7 and competing side reactions. The chemistry of conversion of OH to $HO_2$ is discussed in detail in a later section. Since the concentrations of $H_2O_2$ and $O_3$ were such that the system was optically thin at 248.5 nm, $[OH]_0$ could be calculated from the following relationship

$$[OH]_0 = \Phi_{OH}\sigma(H_2O_2,248.5\ nm,T)[H_2O_2]F \quad (I)$$

where $\Phi_{OH}$ is the quantum yield for OH production from 248.5-nm photolysis of $H_2O_2$, $\sigma(H_2O_2,248.5\ nm,T)$ is the absorption cross section for $H_2O_2$ at 248.5 nm and temperature $T$, and $F$ is the laser photon fluence. The determination of each factor in eq I is discussed in detail below.

$\Phi_{OH}$: It is known[9-11] that $\Phi_{OH} \simeq 2$.

$\sigma(H_2O_2,248.5\ nm,T)$: The absorption cross section for $H_2O_2$ at 248.5 nm is known to be 8.8 × $10^{-20}$ $cm^2$ at 298 K.[8] We have recently measured temperature-dependent absorption cross sections for hydrogen peroxide over the wavelength range 193–350 nm.[12] At 248.5 nm, the following expression describes the observed temperature dependence (units are $cm^2$ $molecule^{-1}$):

$$\sigma(H_2O_2,248.5\ nm,T) = 1.023 \times 10^{-19} \exp\{(-45 \pm 20)/T\} \quad (II)$$

$[H_2O_2]$: Hydrogen peroxide can be lost in the slow-flow system either by decomposition (particularly at higher temperatures) or by condensation (at lower temperatures). To ensure that the $H_2O_2$ concentration in the reactor was known, we monitored $H_2O_2$ by UV photometry before the gas mixture entered the reactor and after the gas mixture exited the reactor. The absorption cells were 216.2 and 90.0 cm in length. The monitoring wavelengths were 228.8 nm in the longer cell (Cd line) and 202.6 nm in the shorter cell ($Zn^+$ line). Both cells were kept at ambient temperature, and the absorption cross sections needed to convert absorbance data to $H_2O_2$ concentration were obtained by interpolation from current NASA recommendations:[8] 1.86 × $10^{-19}$ $cm^2$ at 228.8 nm and 4.31 × $10^{-19}$ $cm^2$ at 202.6 nm. When the reactor temperature was 350 K or below, the difference in $H_2O_2$ concentration measured in the two absorption cells was never more than a few percent. At 391 K, the highest temperature at which experiments were performed, 15–20% of the $H_2O_2$ was lost upon traversal of the reactor. The $H_2O_2$ concentration in the reaction zone was always taken to be the temperature-corrected average of the concentrations measured in the two absorption cells. Under our experimental conditions, absorption by ozone was negligible compared to absorption by $H_2O_2$ at 202.6 nm. At 228.8 nm, ozone made a small but significant contribution to the total absorbance. Care was taken to ensure that $[O_3]$ was constant during the $I$ and $I_0$ measurements required for the $[H_2O_2]$ determination.

(5) Keyser, L. F. *J. Phys. Chem.* **1982**, *86*, 3439.
(6) Ravishankara, A. R.; Wine, P. H.; Nicovich, J. M. *J. Chem. Phys.* **1983**, *78*, 6629.
(7) Brune, Wm. H.; Schwab, J. J.; Anderson, J. G. *J. Phys. Chem.* **1983**, *87*, 4503.
(8) DeMore, W. B.; Margitan, J. J.; Molina, M. J.; Watson, R. T.; Golden, D. M.; Hampson, R. F.; Kurylo, M. J.; Howard, C. J.; Ravishankara, A. R. "Chemical Kinetics and Photochemical Data for Use in Stratospheric Modeling", Evaluation No. 7, JPL Publication 85-37, 1985.
(9) Volman, D. H. *Adv. Photochem.* **1963**, *1*, 43.
(10) Greiner, N. R. *J. Chem. Phys.* **1966**, *45*, 99.
(11) Vaghjiani, G. L.; Ravishankara, A. R., private communication.
(12) Nicovich, J. M.; Wine, P. H., to be submitted for publication.

*F*: The photolysis laser beam was made spatially uniform through use of a segmented aperture optical integrator.[6,13] Virtually the whole cross-sectional area of the cell was irradiated, and the depth of focus of the integrated beam was such that radical concentrations were nearly uniform down the entire length of the cell. The laser beam fluence was measured as the beam exited the reactor by using an EG&G photodiode based radiometer capable of measuring individual pulses. Pulse-to-pulse stability, a requirement for signal averaging in this type of experiment, was found to be very good. Only an occasional pulse energy deviated from the average by more than ±5%. In order to avoid having to correct the measured fluence for reflection off the back window, an antireflection coated window with >99.5% transmission at 248.5 nm was employed. The radiometer was calibrated by using a novel ozone actinometry method which has been described in detail previously.[6]

As mentioned above, all experiments were carried out under slow-flow conditions. The linear flow velocity through the reactor was typically 12 cm $s^{-1}$, and the laser repetition rate was typically 0.4 Hz. The reactor was 23 cm in length, so the reactor volume was completely replenished with a fresh gas mixture between laser pulses. All experiments employed nitrogen as the buffer gas at a total pressure of 80 Torr. Data were obtained over the temperature range 266–391 K. The temperature range was limited at the low end by the vapor pressure of $H_2O_2$ and at the high end by the thermal instability of $H_2O_2$.

The gases used in this study had the following stated minimum purities: $N_2$, 99.999%; $O_2$, 99.99%. Hydrogen peroxide was 90 wt % in water. It was concentrated further by bubbling $N_2$ through the sample for several days before experiments were undertaken and continuously during the course of the experiments. To prevent significant decomposition of $H_2O_2$, all components traversed by $H_2O_2$ between the bubbler and the exit from the last absorption cell were Pyrex or Teflon with the exception of a few stainless steel fittings. The needle valve and flowmeter in the $H_2O_2$ line were positioned so that $N_2$ flowed through these components before entering the bubbler. Ozone was prepared by passing $O_2$ through a commercial ozonator and was stored on silica gel at 197 K. Before use it was degased at 77 K to remove $O_2$. Dilute $O_3/N_2$ mixtures were prepared in 12-L Pyrex bulbs for use in experiments.

A typical experiment was initiated by flowing (3–10) × $10^{12}$ $O_3$ molecules $cm^{-3}$ in 80 Torr of $N_2$ through the reactor and absorption cells. $I_0$ and $J_0$, the intensities of 228.8- and 202.6-nm light transmitted through the absorption cells, were measured. Next, $H_2O_2$ was introduced into the gas flow, the $N_2$ flow was reduced so the total flow rate and total pressure were the same after addition of $H_2O_2$ as before addition of $H_2O_2$, and $I$ and $J$, the reduced intensities of 228.8- and 202.6-nm light transmitted through the reactor, were measured. Using the measured values of $I$, $I_0$, $J$, and $J_0$, we calculated the concentration of $H_2O_2$ in the gas stream entering and exiting the reactor; it ranged from (2–6) × $10^{15}$ molecules $cm^{-3}$. $I$ and $J$ were continuously monitored during the course of an experiment. The multichannel analyzer was pretriggered before the photolysis laser fired to obtain the background count rate. The concentration of $O(^3P)$ was monitored as a function of time after the photolysis pulse. A total of 50–200 laser shots were averaged to obtain one pseudo-first-order kinetic decay. The fluence of each laser pulse was measured by using the radiometer and a calibrated aperture. The laser fluence was varied at constant $[O_3]$ and $[H_2O_2]$ to obtain pseudo-first-order decays as a function of $[HO_2]$. Five to ten fluence values were employed to determine each bimolecular rate constant, $k_1$, from the slope of a $k'$ vs. $[HO_2]$ plot ($k' \equiv$ the $O(^3P)$ pseudo-first-order decay rate). After the fluence variations were completed, the $H_2O_2$ flow was turned off, the total pressure and total flow rate were readjusted, and $I_0$ and $J_0$ were remeasured. All $HO_2$ concentrations employed in the $k_1$ determinations were in the range (0.15–8.5) × $10^{12}$ molecules $cm^{-3}$. It should be noted that, in a series of runs involving variation of the laser fluence at constant $[O_3]$ and $[H_2O_2]$, the ratio $[OH]_0/[O(^3P)]_0$ is not altered; to change this ratio, the composition of the reaction mixture must be varied.

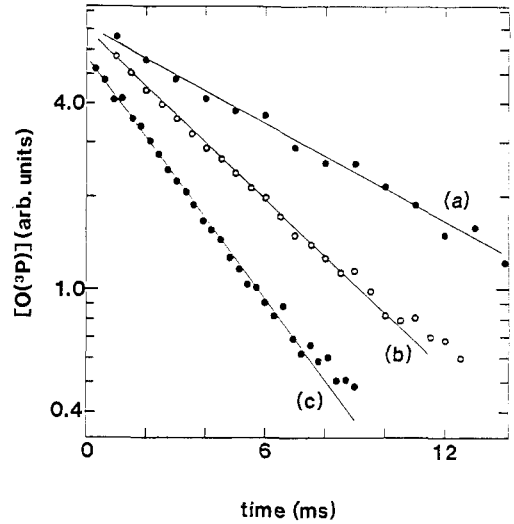


**Figure 2.** Typical $O(^3P)$ temporal profiles observed following 248.5-nm pulsed laser photolysis of $O_3/H_2O_2/N_2$ mixtures. Experimental conditions: $T$ = 281 K, $P$ = 80 Torr, $[H_2O_2]$ = 3.9 × $10^{15}$ molecules $cm^{-3}$, $[O_3]$ = 6 × $10^{12}$ molecules $cm^{-3}$, laser fluence (in units of mJ $cm^{-2}$) = (a) 1.95, (b) 4.55, and (c) 6.31. Solid lines are obtained from least-squares analyses of the first two $1/e$ times of $O(^3P)$ decay and give the following pseudo-first-order decay rates ($k'_{expt}$): (a) 111 $s^{-1}$, (b) 210 $s^{-1}$, (c) 303 $s^{-1}$.

## Results and Discussion

In the absence of competing side reactions which affect the $HO_2$ concentration, the kinetic system is inherently pseudo-first-order; i.e., all $HO_2$ lost via reaction 1 is rapidly regenerated via reaction 7. However, as will be discussed in detail below, the importance of certain side reactions is suppressed when $[HO_2] \gg [O(^3P)]$. Most of our experiments were carried out under experimental conditions where $[HO_2] \approx 10[O(^3P)]_0$, although this ratio was varied as a check on the kinetic model used to extract $k_1$. At low temperature, where relatively low $H_2O_2$ concentrations had to be employed, the $HO_2$ to $O(^3P)$ ratio was typically somewhat lower than that employed at higher temperatures.

Photolytically produced $O(^3P)$ can be lost via the following (pseudo) first-order processes:

$$O(^3P) + HO_2 \rightarrow OH + O_2 \quad (1)$$

$$O(^3P) + H_2O_2 \rightarrow OH + HO_2 \quad (9)$$

$$O(^3P) + O_3 \rightarrow 2O_2 \quad (10)$$

$$O(^3P) \rightarrow \text{loss by diffusion from the detector field of view and reaction with background impurities} \quad (11)$$

Under our experimental conditions, reaction 1 dominated $O(^3P)$ removal except at very low $HO_2$ levels. Reaction 10 was of negligible importance while reaction 9 was minor but not negligible.[14] $k_{11}$ was directly measured to be ~5 $s^{-1}$—1–2 orders of magnitude slower than $k_1[HO_2]$ under most experimental conditions.

In the absence of competing side reactions which affect the concentrations of $O(^3P)$ or $HO_2$, removal of $O(^3P)$ should obey first-order kinetics

$$\ln \{[O(^3P)]_0/[O(^3P)]\} = (k_1[HO_2] + k_d)t \equiv k'_{expt}t \quad (III)$$

where

$$k_d \equiv k_9[H_2O_2] + k_{10}[O_3] + k_{11} \quad (IV)$$

(13) Ravishankara, A. R.; Eisele, F. L.; Kruetter, N. M.; Wine, P. H. *J. Chem. Phys.* **1981**, *74*, 2267.

(14) Wine, P. H.; Nicovich, J. M.; Thompson, R. J.; Ravishankara, A. R. *J. Phys. Chem.* **1983**, *87*, 3948.

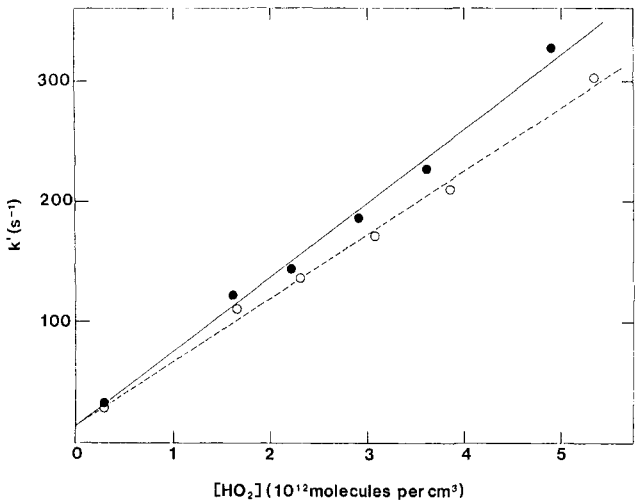


**Figure 3.** Typical plots of $k'_{exptl}$ vs. $[OH]_0$ (open circles) and $k'$ vs. $[HO_2]_{max}$ (closed circles). Experimental conditions: $T = 281$ K, $P = 80$ Torr, $[H_2O_2] = 3.9 \times 10^{15}$ molecules $cm^{-3}$, $[O_3] = 6 \times 10^{12}$ molecules $cm^{-3}$. The dashed line is obtained from a linear least-squares analysis of the $k'_{exptl}$ vs. $[OH]_0$ data and gives the "uncorrected" rate coefficient $(5.24 \pm 0.38) \times 10^{-11}$ $cm^3$ $molecule^{-1}$ $s^{-1}$. The solid line is obtained from a linear least-squares analysis of the $k'$ vs. $[HO_2]_{max}$ data and gives the "corrected" rate coefficient $(6.15 \pm 0.54) \times 10^{-11}$ $cm^3$ $molecule^{-1}$ $s^{-1}$.

**TABLE I: Reaction Set for Computer Simulations**

| reaction | rate coefficient[a,b] |
|---|---|
| $O + HO_2 \rightarrow OH + O_2$ | $k_1 = 3 \times 10^{-11} \exp(200/T)$ |
| $O + OH \rightarrow H + O_2$ | $k_2 = 2.2 \times 10^{-11} \exp(117/T)$ |
| $H + O_3 \rightarrow OH + O_2$ | $k_4 = 1.4 \times 10^{-10} \exp(-470/T)$ |
| $OH + H_2O_2 \rightarrow HO_2 + H_2O$ | $k_7 = 3.1 \times 10^{-12} \exp(-187/T)$ |
| $O + H_2O_2 \rightarrow OH + HO_2$ | $k_9 = 1.4 \times 10^{-12} \exp(-2000/T)$ |
| $O + O_3 \rightarrow 2O_2$ | $k_{10} = 8 \times 10^{-12} \exp(-2060/T)$ |
| $O \rightarrow$ loss | $k_{11} = 5\ s^{-1}$ |
| $OH + HO_2 \rightarrow O_2 + H_2O$ | $k_{12} = 1.7 \times 10^{-11} \exp(416/T) + 3 \times 10^{-31}[M] \exp(500/T)$ |
| $HO_2 + HO_2 \rightarrow H_2O_2 + O_2$ | $k_{13} = 2.3 \times 10^{-13} \exp(590/T) + 1.7 \times 10^{-33}[M] \exp(1000/T)$ |
| $HO_2 \rightarrow$ loss | $k_{14} = 5\ s^{-1}$ |
| $HO_2 + O_3 \rightarrow OH + 2O_2$ | $k_{15} = 1.4 \times 10^{-14} \exp(-580/T)$ |
| $H + HO_2 \rightarrow 2OH$ | $k_{16a} = 6.4 \times 10^{-11} \exp(0/T)$ |

[a] All rate coefficients are taken from ref 9 except $k_{11}$ which was measured and $k_{14}$ which was set equal to $k_{11}$. [b] All rate coefficients except $k_{11}$ and $k_{14}$ are in units of $cm^3$ $molecule^{-1}$ $s^{-1}$.

Figure 2 shows typical plots of ln $[O(^3P)]$ vs. $t$. Equation III does indeed appear to be obeyed. If side reactions were unimportant, the bimolecular rate coefficient would be obtained from the slope of a $k'_{exptl}$ vs. $[OH]_0$ plot, such as shown in Figure 3.

*Secondary Chemistry.* In the paper describing our 298 K study of reaction 1, possible side reactions were considered in detail.[6] It was concluded that two reactions could significantly affect the $HO_2$ temporal profile:

$$OH + HO_2 \rightarrow O_2 + H_2O \quad (12)$$

$$HO_2 + HO_2 \rightarrow H_2O_2 + O_2 \quad (13)$$

To quantify the roles of reactions 12 and 13 in our kinetics experiments, a series of computer simulations were carried out where the temporal profiles of key species were calculated under a variety of experimental conditions by numerical integration of the appropriate rate equations. For completeness, a number of reactions which were expected to play very minor roles in the $O(^3P)$ and $HO_2$ kinetics were included in the mechanism. The complete sets of reactions and rate coefficients used in the simulations are given in Table I.

Reaction 12 competes with reaction 7 during the period immediately after the laser pulse when OH is being converted to $HO_2$. Each time reaction 12 occurs, two $HO_2$ radicals are lost which otherwise would have been present to react with $O(^3P)$. Reaction 12 is most important at high laser fluence (i.e., high

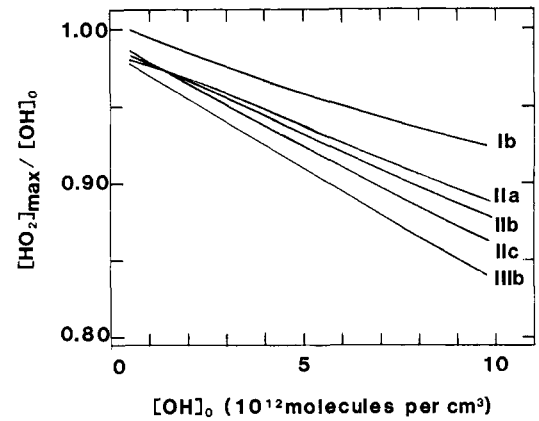


**Figure 4.** Typical correction curves (obtained from computer simulations) which relate $[HO_2]_{max}$ to $[OH]_0$. All curves shown in the figure are from simulations with $[H_2O_2] = 4 \times 10^{15}$ molecules $cm^{-3}$. Temperature: I, 400 K; II, 300 K; III, 260 K. $[OH]_0/[O(^3P)]_0$: a, $10^4$; b, 10; c, 4.

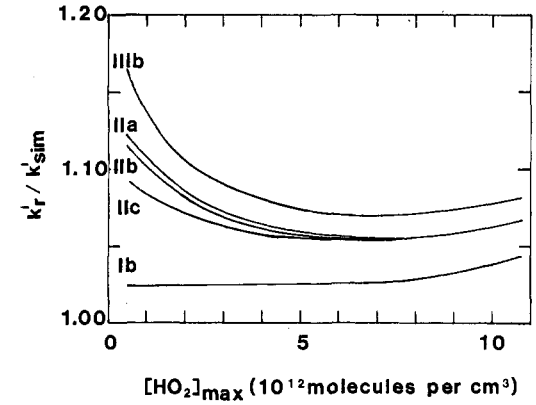


**Figure 5.** Typical correction curves (obtained from computer simulations) which relate $k'_{exptl}$ to $k'$ via eq VI. All curves shown in the figure are from simulations with $[H_2O_2] = 4 \times 10^{15}$ molecules $cm^{-3}$. Temperature: I, 400 K; II, 300 K; III, 260 K. $[OH]_0/[O(^3P)]_0$: a, $10^4$; b, 10; c, 4.

$[OH]_0/[H_2O_2]$) and at low temperature. From the computer simulations, a set of curves were constructed which relate $[HO_2]_{max}$, the peak amount of $HO_2$ present after all photolytically produced OH has reacted away but before appreciable $HO_2$ loss via processes such as reaction 13 has occurred, to $[OH]_0$. Representative correction curves are plotted in Figure 4. For the 101 experiments used in the $k_1(T)$ determinations, the average value for $[HO_2]_{max}/[OH]_0$ was 0.947 while the minimum value under any set of experimental conditions was 0.845.

As pointed out above, loss of $O(^3P)$ via reactions 1 and 9–11 occurs on a time scale which is long compared to the time scale for $HO_2$ formation. Hence, if the concentration of $HO_2$ were constant over the time period of $O(^3P)$ removal, $k_1$ could be obtained from the slope of a $k'_{exptl}$ vs. $[HO_2]_{max}$ plot. Unfortunately, small but significant time variation of $[HO_2]$ can result from the occurrence of reactions 9, 13, and 14. Reactions 9 and

$$HO_2 \rightarrow \text{loss by diffusion from the reaction zone and reaction with background impurities} \quad (14)$$

14 are most important at low laser fluences, i.e., low $[HO_2]$. Reaction 9 is strongly temperature dependent and increases in importance at high temperature. Reaction 9 is also a more important source of $HO_2$ when $[OH]_0/[O(^3P)]_0$ is relatively low. Reaction 13 becomes an important $HO_2$ removal mechanism at relatively high $HO_2$ concentrations. To avoid large corrections for $HO_2$ loss via reaction 13, all experiments were carried out with $[HO_2]_{max} < 9 \times 10^{12}$ molecules $cm^{-3}$ and all data analyses were restricted to two $1/e$ times of $O(^3P)$ decay; i.e., no data where $[O(^3P)]/[O(^3P)]_0 < 0.13$ were used in the data analysis. Computer simulations were carried out under a variety of experimental

**TABLE II: Summary of Our O + $HO_2$ Kinetic Data**

| $T$, K | no. of expts[a] | $[H_2O_2]$, $10^{15}$ cm$^{-3}$ | $[OH]_0/[O]_0$ | range of $k'$, s$^{-1}$ | $k_1$, $10^{-11}$ cm$^3$ molecule$^{-1}$ s$^{-1}$, $\pm 2\sigma$[b] uncorrected[c] | corrected[d] |
|---|---|---|---|---|---|---|
| 266 | 6 | 2.98 | 5.0 | 100–268 | 5.22 ± 0.51 | 7.00 ± 0.70 |
| 266 | 6 | 2.37 | 6.8 | 28–209 | 5.92 ± 0.39 | 7.14 ± 0.52 |
| 275 | 6 | 5.61 | 12 | 57–608 | 5.58 ± 0.54 | 6.60 ± 0.75 |
| 281 | 6 | 3.90 | 11 | 33–327 | 5.24 ± 0.38 | 6.15 ± 0.54 |
| 298 | 5 | 4.22 | 10 | 56–558 | 5.29 ± 0.65 | 6.30 ± 0.91 |
| 300 | 10 | 3.57 | 7.1–17 | 51–487 | 5.16 ± 0.30 | 6.16 ± 0.73 |
| 300 | 6 | 2.05 | 6.8 | 32–293 | 5.21 ± 0.73 | 6.34 ± 0.73 |
| 300 | 7 | 3.81 | 6.9 | 66–358 | 4.81 ± 0.52 | 5.69 ± 0.56 |
| 318 | 6 | 5.46 | 13 | 73–547 | 5.48 ± 0.13 | 6.28 ± 0.09 |
| 328 | 8 | 3.07 | 8.0 | 66–326 | 5.44 ± 0.24 | 6.24 ± 0.28 |
| 354 | 6 | 3.90 | 16 | 55–418 | 5.14 ± 0.45 | 5.86 ± 0.54 |
| 359 | 5 | 4.63 | 15 | 92–368 | 4.52 ± 0.69 | 5.11 ± 0.70 |
| 374 | 8 | 4.62 | 15 | 75–361 | 4.40 ± 0.40 | 4.87 ± 0.43 |
| 380 | 7 | 4.71 | 19 | 72–466 | 5.11 ± 0.39 | 5.63 ± 0.40 |
| 391 | 9 | 4.94 | 11 | 111–438 | 4.87 ± 0.32 | 5.28 ± 0.38 |

[a] Experiment ≡ determination of one pseudo-first-order rate coefficient. [b] Errors represent precision only. [c] Obtained from the slopes of $k'_{exptl}$ vs. $[OH]_0$ plots. [d] Obtained from the slopes of $k'$ vs. $[HO_2]_{max}$ plots.

**TABLE III: Comparison of Our Results with Those of Other Investigators**

| range of $T$, K | range of $P$, Torr | M | exptl method[a] | exptl conditions | $A$[b] | $E/R$, K | $k_1$ (298 K)[b] | ref |
|---|---|---|---|---|---|---|---|---|
| 298 | 1.0 | He | DF–LMR | relative to $k_2$ | | | 2.7 ± 1.0[c] | 1 |
| | | | | relative to $k_7$ | | | 6.3 ± 2.0[c] | |
| 298 | 0.8–2.3 | He | DF–LMR/ESR | $[O(^3P)] \gg [HO_2]$ | | | 3.7 ± 1.1 | 2 |
| | 2.8–3.4 | | | $[HO_2] \gg [O(^3P)]$ | | | 4.2 ± 1.5 | |
| | 3.7–5.5 | | | relative to $k_2$ | | | 3.0 ± 0.9[c] | |
| 298 | 1200 | $Ar/H_2/O_2$ | PR–UVA | $k_1$ extracted by modeling complex chemistry | | | 7 ± 2 | 3 |
| 296 ± 2 | 2.5 | He | DF–RF/LIF | $[HO_2] \gg [O(^3P)]$ | | | 5.4 ± 0.9 | 4 |
| 229–372 | 1.0 | He | DF–RF | $[HO_2] \gg [O(^3P)]$ | 3.1 ± 0.3 | 200 ± 28 | 6.1 ± 0.4 | 5 |
| 298 | 10–500 | $N_2$ | PLP–RF | $[HO_2] \gg [O(^3P)]$ | | | 6.1 ± 1.1[d] | 6 |
| 300 | 1.0–4.0 | He | DF–LMR/RF/RA | $[O(^3P)] \gg [HO_2]$ | | | 5.2 ± 0.8 | 7 |
| | | | | $[HO_2] \gg (O(^3P)]$ | | | | |
| 266–391 | 80 | $N_2$ | PLP–RF | $[HO_2] \gg [O(^3P)]$ | 2.9 ± 0.7 | 228 ± 75 | 6.2 ± 1.0 | this work. |

[a] DF, discharge flow; LMR, laser magnetic resonance; ESR; electron spin resonance; PR, pulsed radiolysis; UVA, ultraviolet absorption; RF, resonance fluorescence; LIF, laser-induced fluorescence; PLP, pulsed laser photolysis; RA, resonance absorption. [b] Units are $10^{-11}$ cm$^3$ molecule$^{-1}$ s$^{-1}$. [c] $k_1$ recalculated with presently recommended (ref 9) values for the reference reactions. [d] Corrected downward from reported value by 1.5% to account for small change in recommended $H_2O_2$ absorption cross section.

conditions. The first two $1/e$ times of the slightly nonexponential computer generated $O(^3P)$ temporal profiles were least squares fit to an exponential decay to obtain $k'_{sim}$, the simulated decay rate. The simulated decay rates were then compared to the "real" decay rates, $k'_r$, to obtain a set of correction curves, some of which

$$k'_r \equiv k_1[HO_2]_{max} + k_9[H_2O_2] + k_{10}[O_3] + k_{11} \quad (V)$$

are shown in Figure 5. The first two $1/e$ times of each experimental $O(^3P)$ temporal profile were least squares fit to eq III to obtain $k'_{exptl}$. A corrected value of $k'$ was then computed from the expression

$$k' = k'_{exptl}(k'_r/k'_{sim}) \quad (VI)$$

One source of uncertainty in the computer simulations concerns the fact that $k_{14}$ was not measured; it was estimated that $k_{14} = k_{11} \approx 5$ s$^{-1}$. Lack of knowledge of the exact value of $k_{14}$ increases the uncertainty in the $k'_r/k'_{sim}$ factors at low concentrations of $HO_2$. The low $[HO_2]$ data are relatively unimportant in defining $k_1$, so the uncertainty in $k_{14}$ makes only a minor contribution to the overall uncertainty in $k_1$. For the 101 experiments used in the $k_1(T)$ determinations, the average value of $k'_r/k'_{sim}$ was 1.06 and the maximum value under any set of experimental conditions was 1.18.

As discussed above, $k_1$ values corrected for secondary chemistry were obtained from the slopes of plots of $k'$ vs. $[HO_2]_{max}$. Typical data are shown in Figure 3. For all 15 rate coefficients measured, the corrected $k_1$ values were larger than the values which would have been obtained from plots of $k'_{exptl}$ vs. $[OH]_0$ (see Figure 3, for example). The magnitude of the secondary chemistry corrections was largest at the lowest temperatures. For the 15 rate coefficients reported, the average difference between the corrected and uncorrected bimolecular rate coefficients was 16% while the largest difference was 26%.

*Summary of Results.* The experimental results are summarized in Table II. Errors quoted for individual "corrected" $k_1$ determinations are $2\sigma$ and refer only to the precision of the $k'$ vs. $[HO_2]_{max}$ data. The absolute accuracy of our $k_1$ determinations is limited not only by precision but also by uncertainties in measurement of the laser photon fluences ($F$), the $H_2O_2$ concentration, the correction factor used to obtain $[HO_2]_{max}$ from $[OH]_0$, the correction factor used to obtain $k'$ from $k'_{exptl}$ (i.e., $k'_r/k'_{sim}$), and unidentified systematic errors. We estimate the pertinent $2\sigma$ uncertainties to be as follows: $F$, 10%; $[H_2O]$, 5%; $[HO_2]_{max}/[OH]_0$, 5%; $k'_r/k'_{sim}$; 10% at 266 K and 5% at 298 K and above; unidentified systematic errors, 5%. Precision did not appear to be temperature dependent and averaged 9%. Hence, the absolute accuracy of an individual $k_1$ determination is estimated to be ±23% at 266 K and ±21% at 298 K and above.

An Arrhenius plot of our results is shown in Figure 6. An unweighted linear least-squares analysis of the ln $k_1$ vs. $1/T$ data gives the following expression (units are cm$^3$ molecule$^{-1}$ s$^{-1}$):

$$k_1(T) = (2.91 \pm 0.70) \times 10^{-11} \exp[(228 \pm 75)/T] \quad (VII)$$

The uncertainties quoted in the above expression are $2\sigma$ and represent precision only.

*Comparison with Previous Work.* Our results are compared with those reported by other investigators in Table III. The 298 K value reported in this paper is identical with our previously reported value[6] and at the upper end of the group of recent direct determinations[4-7] which span the range (5.2–6.2) × $10^{-11}$ cm$^3$ molecule$^{-1}$ s$^{-1}$. Other than our studies, the other recent direct measurements all employed low-pressure discharge flow systems,

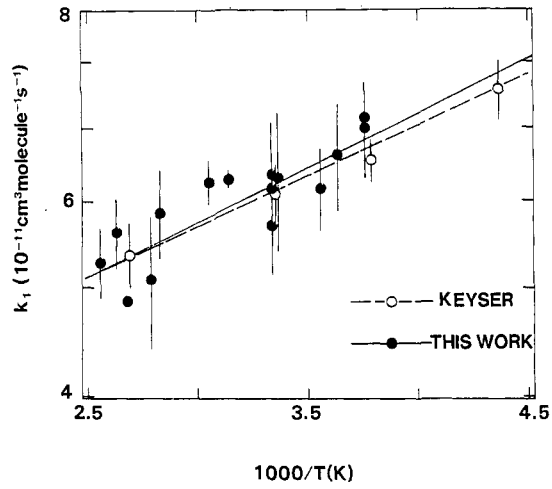


**Figure 6.** Arrhenius plot for the O + $HO_2$ reaction.

all measured not only $O(^3P)$ but also $HO_2$ (either directly or indirectly by conversion to OH), and all carefully considered the role of competing side reactions. Hence, there is no obvious reason to prefer one value over another. The early work of Burrows et al.[1] and Hack et al.[2] give $k_1$(298 K) values which are considerably lower than those reported in ref 4–7. Possible reasons for the apparently erroneous results reported in ref 1 and 2 are discussed elsewhere.[5] Lii et al.[3] obtained a value for $k_1$ by comparing computer simulations with $HO_2$ and $O_3$ concentration profiles observed following pulsed radiolysis of $O_2$–$H_2$–Ar mixtures. Their reported rate coefficient agrees well with our results. However, as pointed out by Keyser,[5] the experimental data of Lii et al. are very insensitive to the value of $k_1$; hence, their error limits should be ~500% rather than the reported 30%.

Very little temperature-dependent data are available for reaction 1. Values for $k_1$ of $8 \times 10^{-11}$ cm$^3$ molecule$^{-1}$ s$^{-1}$ at 1600 K[15] and $6 \times 10^{-11}$ cm$^3$ molecule$^{-1}$ s$^{-1}$ at 1050 K[16] have been inferred from flame studies. The only previous temperature dependence study in the atmospheric temperature regime is that of Keyser.[5] As seen from the comparisons in Table III and Figure 6, our results are in excellent agreement with those of Keyser. Since our experiments were very different in methodology from Keyser's and are subject to different sources of systematic errors, the uncertainty of $k_1(T)$ for atmospheric modeling purposes is now greatly reduced. Keyser's study employed helium buffer gas at a pressure of 1.0 Torr while our study employed nitrogen buffer gas at a pressure of 80 Torr. Thus, agreement between the two studies strongly suggests that $k_1$ is independent of pressure over the relevant upper atmospheric temperature and pressure ranges.

Reaction 1 could proceed via a hydrogen abstraction mechanism (1a) or via formation of an energized HOOO "pseudo-intermediate" (1b):

$$O + HO_2 \rightarrow O\cdots HO_2 \rightarrow OH + O_2 \quad (1a)$$

$$O + O_2H \rightarrow O\cdots OOH \rightarrow O_2 + OH \quad (1b)$$

Sridharan et al.[17] recently reported an elegant experiment in which $^{16}OH$ and $^{18}OH$ products from the reaction of $^{18}O$ with $HO_2$ were monitored in a discharge flow system. They found that only $^{16}OH$ was produced, implying that O reacts with $HO_2$ via channel 1b. Thermochemical estimates suggest that HOOO is bound relative to O + $HO_2$ but is ~12 kcal mol$^{-1}$ less stable than the OH + $O_2$ products.[18,19] Mozurkewich[20] points out that since HOOO is bound relative to O + $HO_2$, we might expect to find a long-range interaction that would produce a transition state for reaction 1 very similar to that expected for formation of HOOO. Mozurkewich's RRKM calculations yield a rate constant for formation of HOOO of $5.5 \times 10^{-11}$ cm$^3$ molecule$^{-1}$ s$^{-1}$, independent of temperature.[20] The observed negative activation energy for reaction 1 could probably be reproduced if a small barrier were assumed in the HOOO → OH + $O_2$ reaction path.[21]

*Implications for Atmospheric Chemistry.* Model calculations of OH and $HO_2$ concentration profiles in the upper stratosphere are very sensitive to the choice of $k_1(T)$. Kaye and Jackman,[22] considering both sensitivity of their model to various parameters and uncertainties in these parameters, have concluded that the uncertainty of $k_1$ contributes more to the uncertainty in [OH] and [$HO_2$] at 35° N, 40-km altitude than any parameter in their model except $k_{12}$. The currently recommended value[8] for $k_1(T)$ is

$$k_1(T) = 3.0 \times 10^{-11} \exp[(200 \pm 200)/T] \text{ cm}^3 \text{ molecule}^{-1} \text{ s}^{-1} \quad \text{(VIII)}$$

The results reported in this paper will have little effect on the recommended $A$ factor and activation energy but will substantially reduce the uncertainty in the above expression; this will, in turn, significantly reduce the overall uncertainty in model calculations of upper stratospheric OH and $HO_2$ concentrations and facilitate meaningful comparisons of stratospheric measurements with photochemical models.

Jackman et al.[23] have recently compared $O_3$ concentrations at 5° N and 43-km altitude measured by LIMS (limb infrared monitor of the stratosphere) with those calculated from a photochemical model using LIMS measurements of $H_2O$, $HNO_3$, and $NO_2$ and temperature and SAMS (stratospheric and mesospheric sounder) measurements of $CH_4$ as input. The model predicted lower $O_3$ levels than those actually observed. A sensitivity analysis showed that the overall uncertainty in the model calculation was a factor of 1.7, about the same magnitude as the discrepancy between model and measurement. Of the many parameters used in the model, the uncertainty of $k_1$ was found to make the sixth largest contribution to the overall uncertainty of the calculation. Our results will therefore result in a small but significant reduction in the model uncertainty.

*Acknowledgment.* This work was supported by the National Aeronautics and Space Administration through Subcontract 954814 from the Jet Propulsion Laboratory and Grant NAGW 1001.

(15) Peeters, J.; Mahnen, G. *Symp. (Int.) Combust., [Proc.]* **1972**, *14*, 133.
(16) Day, M. J.; Thompson, K.; Dixon-Lewis, G. *Symp. (Int.) Combust., [Proc.]* **1972**, *14*, 47.
(17) Sridharan, U. C.; Klein, F. S.; Kaufman, F. *J. Chem. Phys.* **1985**, *82*, 592.
(18) Nangia, P. S.; Benson, S. W. *J. Phys. Chem.* **1979**, *83*, 1138.
(19) Benson, S. W. *Oxid. Commun.* **1982**, *2*, 169.
(20) Mozurkewich, M. *J. Phys. Chem.* **1986**, *90*, 2216.
(21) Mozurkewich, M.; Benson, S. W. *J. Phys. Chem.* **1984**, *88*, 6429.
(22) Kaye, J. A.; Jackman, C. H. *J. Geophys. Res.* **1986**, *91*, 1117.
(23) Jackman, C. H.; Stolarski, R. S.; Kaye, J. A. *J. Geophys. Res.* **1986**, *91*, 1103.